Contents lists available at ScienceDirect

Nuclear Instruments and Methods in Physics Research A

Design and characterization of permanent magnetic solenoids for REGAE

M. Hachmann [a,*], K. Flöttmann [a], T. Gehrke [b], F. Mayet [a]

[a] Deutsches Elektronen-Synchrotron DESY, Notkestraße 85, 22607 Hamburg, Germany
[b] Deutsches Krebsforschungszentrum DKFZ, Im Neuenheimer Feld 280, 69120 Heidelberg, Germany

ARTICLE INFO

ABSTRACT

REGAE is a small electron linear accelerator at DESY. In order to focus short and low charged electron bunches down to a few μm permanent magnetic solenoids were designed, assembled and field measurements were done. Due to a shortage of space close to the operation area an in-vacuum solution has been chosen. Furthermore a two-ring design made of wedges has been preferred in terms of beam dynamic issues. To keep the field quality of a piecewise built magnet still high a sorting algorithm for the wedge arrangement including a simple magnetic field model has been developed and used for the construction of the magnets. The magnetic field of these solenoids has been measured with high precision and compared to simulations.

1. Introduction

The Relativistic Electron Gun for Atomic Exploration (REGAE) is a small 5 MeV linear accelerator at DESY in Hamburg, which produces short, low emittance electron bunches. It originally was meant for temporal resolving electron diffraction experiments [1,2] only, but two further experiments are currently planned at REGA. First, an external injection experiment for Laser Wakefield Acceleration (LWA) [3] will be performed in the framework of the LAOLA collaboration (LAboratory fOr Laser- and beam-driven plasma Acceleration). Second, as extension of the original experiment, a time resolved high energy Transmission Electron Microscope (TEM) will be set up.

Both experiments require two strong focusing magnets inside a new target chamber before and after the respective targets. Permanent magnetic solenoids (PMS) can provide the needed focusing strength due to their enormous surface current density, while having compact dimensions at the same time. Since short and strong solenoids, as required, exhibit a distinct non-linearity, the induced emittance growth is comparatively large and has to be minimized as far as possible. Furthermore, the focusing strength is not adjustable and 3D in-vacuum movers are required for positioning the magnets. Due to the chosen movers a weight limitation for the magnets reveals as an additional requirement. Overcoming these difficulties PMS are an interesting alternative if a low energy beam has to be strongly focused.

2. Design

A strong focusing down to a few μm is needed for the external injection experiment as well as for a large magnification of the TEM. The investigations of different designs have shown that a solenoid has to be as close as possible to the target position in order to achieve the required transverse beam sizes. Besides, a comparably large target chamber (diameter of 60 cm) for different experiments is required. Hence we decided to go for a in-vacuum solution. Furthermore, taking a weight limitation of $m < 1$ kg due to the in-vacuum movers into account a solenoid consisting of two radially magnetized rings should be preferred over a single axially magnetized ring [4]. A higher magnetic field and therefore a larger focus strength as well as a smaller induced emittance growth can be achieved since a two-ring design allows a larger influence on the field shape (adjustable distance between both rings $d = 2\,l_1$; see Fig. 1). In the particular case at REGAE, a reduction of the emittance growth by 65% is feasible. The PMS dimensions (in mm) depicted in Fig. 1 are as follows $R_o = 25.4$, $R_i = 17$, $l_1 = 7.8$ and $l_2 = 44.8$ while the weight is just $m = 0.628$ kg. The focal length of a REGAE-like electron beam (5 MeV) is ~ 0.2 m and transverse beam sizes of a few μm are achievable. The two radially magnetized ring design fulfills all asked demands. A more detailed presentation of the design can be found in [4]. For technical reasons radially magnetized rings need to be assembled from wedges. We decided for 12 wedges per ring as compromise of field symmetry and manufacturing aspects. The wedges are neodymium magnets (NdFeB). The imperfections of the wedges call for a sorting algorithm in order to preserve the field quality.

* Corresponding author.
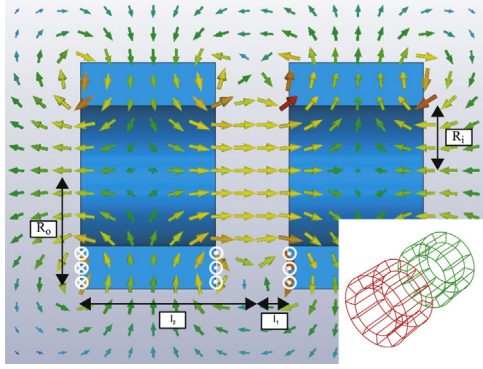 E-mail address: max.hachmann@desy.de (M. Hachmann).

Fig. 1. CST magnetic field simulation of two radially magnetized rings (blue) and the conceptional wedge-based design (lower right). (For interpretation of the references to color in this figure caption, the reader is referred to the web version of this paper.)
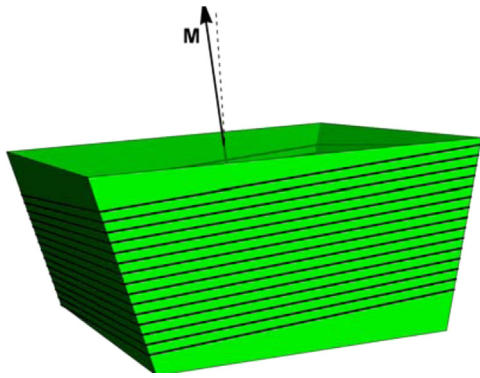

Fig. 2. Current loops model of a flawed wedge with a tilted magnetization.

3. Field description and sorting algorithm

3.1. Field model

Due to the necessity of a model which describes the resulting field of 2×12 wedges we go for a simple analytical approach: each wedge is shaped by current loops covering the surface (Fig. 2), where each loop again can be divided into four straight parts. Each straight part can be described by *Biot–Savart's law* with the result that the magnetic field of a wedge $\mathbf{B}(\mathbf{r})$ follows as

$$\mathbf{B}(\mathbf{r}) = \sum_{i=1}^{N} \sum_{j=1}^{4} \left(\frac{\mu_0}{4\pi} \int_{l_{ij}} I \frac{\mathbf{r} - \mathbf{r}'}{|\mathbf{r} - \mathbf{r}'|^3} \times \mathrm{d}\mathbf{l} \right) \quad (1)$$

where $\mathbf{r}$ denotes the position of the field and $\mathbf{r}'$ the position of a wire element. I is the current and $\mathrm{d}\mathbf{l}$ is the length of the differential element of the wire in the direction of the current. N is the number of current loops, i and j denote the specific current loop and a certain straight line, respectively.

The magnetization $\mathbf{M}$ of a wedge is defined by the direction and its magnitude which were measured by the manufacturer and can be translated into a tilt of the current loops or a variation of the current I, respectively. These transformations have to be introduced to Eq. (1). The mean current over all wedges is chosen in a way that it reproduces the measured maximum longitudinal magnetic field. The manufacturing errors of the magnetization strength are added in proportion to this average current.

The model ignores inhomogeneous magnetization and the relative permeability ($\mu_r \leq 1.05$) of the wedges.

3.2. Sorting algorithm

Since the total magnetic field of the two-ring setup is simply given as the superposition of the individual magnetic fields of the flawed wedges an optimal configuration of the 24 wedges can be found which keeps the transverse beam quality. Due to the absence of a common quantity which expresses the field goodness of a solenoid we have introduced a new one which is proportional to changes of the beam quality due to the magnetic field quality. It is motivated by the *normalized 4D-transverse emittance*:

$$\epsilon_{4D}^2 \sim \begin{vmatrix} \langle x^2 \rangle & \langle x p_x \rangle & \langle xy \rangle & \langle x p_y \rangle \\ \langle x p_x \rangle & \langle p_x^2 \rangle & \langle y p_x \rangle & \langle p_x p_y \rangle \\ \langle xy \rangle & \langle y p_x \rangle & \langle y^2 \rangle & \langle y p_y \rangle \\ \langle x p_y \rangle & \langle p_x p_y \rangle & \langle y p_y \rangle & \langle p_y^2 \rangle \end{vmatrix}. \quad (2)$$

The normalized 4D-transverse emittance takes all kinds of correlations between the four transverse beam quantities $\{\langle x \rangle, \langle y \rangle, \langle p_x \rangle, \langle p_y \rangle\}$ into account, where $\langle x \rangle$ and $\langle y \rangle$ are the transverse RMS beam sizes and $\langle p_x \rangle$ and $\langle p_y \rangle$ are the transverse RMS momentum spreads. The remaining entries are their correlations. To connect the transverse electron bunch phase space with the magnetic field the Lorentz force is calculated. The line integrals of the magnetic field of the PMS parallel to the longitudinal field axis are correlated to the induced transverse momenta:

$$p_x \sim - \int_a^b B_y(z) \, \mathrm{d}z \quad \text{and} \quad p_y \sim \int_a^b B_x(z) \, \mathrm{d}z,$$

where the distance between a and b describes the integration length. The line integrals imply a constant position. From the set of line integrals at different positions (analogous to a particle distribution's phase space) it is possible to calculate a 4D-emittance-like quantity which expresses the degradation of the beam quality in dependence of the field quality.

Using the computationally simple field description and the 4D-emittance-like fitness quantity an evolutionary algorithm has been developed with the goal to find the optimal permutation for each ring given the measured magnetization data provided by the manufacturer. A direct calculation of all permutations ($1 \, \text{PMS} \rightarrow 12! \times 12! \approx 2 \times 10^{17}$; excl. spare wedges and flipping) is not feasible. The algorithm is a two-step process. The first step consists of a numerical least-square algorithm, which determines a rough starting point for the second part. Here all available wedges – including spare wedges (pool) – are taken into account. In each iteration three actions can be performed: swap with pool, swap inside the rings, flip around radial axis.

The second step is based on the concept of *simulated annealing* [5,6]. Simulated annealing tries to find the global minimum of a fitness quantity $Q(x)$ like Eq. (2) by treating the system as a thermodynamical system with falling temperature T. For each iteration $Q(x)$ is determined. Also T is lowered according to a predefined sequence. In our case each iteration consists of *swapping* wedges inside the rings or *flipping* them. x corresponds to a certain permutation of both rings whereas x_{opt} is the current best solution. If $Q(x) \leq Q(x_{opt})$, $x_{opt} = x$. If $Q(x) > Q(x_{opt})$, $x_{opt} = x$ with a probability

$$\exp\left(-\frac{Q(x_{opt}) - Q(x)}{T} \right).$$

Thus for low temperatures T the probability of choosing the permutation decreases, whereas for high T the algorithm tends to *jump* out of minima more often. This helps to avoid trapping in local minima.
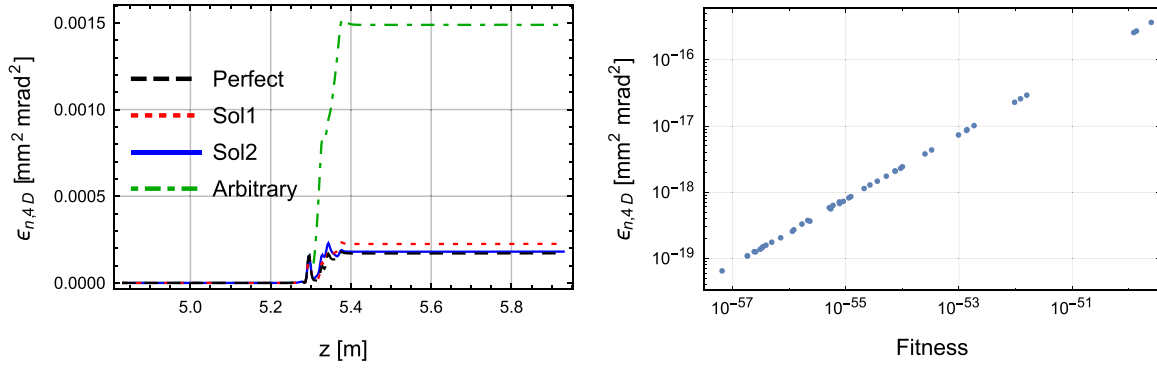
Fig. 3. *Left*: Growth of normalized 4D emittance of different PMS assemblies. The PMS's center is placed at $z = 5.33$ m. *Right*: Correlation between the fitness quantity used for the numerical sorting algorithm and the normalized 4D emittance.

3.3. Results

The best arrangement provided by the algorithm was used to determine emittance growth. Full 3D field maps were calculated for both the flawed and flawless wedge case using the analytical field model in order to do particle tracking using ASTRA [7]. Because the emittance growth depends on the initial beam parameters the results are only valid and comparable for the chosen parameters. Using a 5 MeV beam with an RMS beam size of 610 μm two independent assemblies for two PMS (Fig. 3, left) were found with a relative 4D emittance growth $\epsilon_{flawed}/\epsilon_{flawless}$ of 1.32 and 1.05, respectively. An arbitrary assembly reaches a relative emittance growth of ~ 8.71. Furthermore a strict correlation between the fitness quantity and the normalized 4D emittance could be shown. In Fig. 3 (right) the 4D emittance growth of 22 assemblies were calculated and correlated with their fitness quantity.

4. Field measurement

4.1. 3D-Hall probe

Measuring the magnetic field of a geometrical small magnet with a high precision is challenging. In order to compare the field simulations with a measurement we decided for the Metrolab Three-axis Hall Magnetometer THM1176-HF [8] which provides the required accuracy. With a sensor housing of 5.1 mm × 1.3 mm the geometrical dimensions of the probe are small enough to measure the magnetic field inside the PMS. Furthermore its small active volume of $(150 \times 150 \times 10)$ μm^3 is sufficient to measure the absolute field despite the high field gradients. The Hall probe was calibrated relatively to an NMR Teslameter. The absolute as well as the relative accuracy meet our requirements of 10^{-4}. From a linear regression of the absolute accuracy measurement follows for the slope 0.99998 ± 0.00009 and for the offset $(1.08 \pm 0.03)10^{-4}$.

4.2. Magnetic field measurement and post-processing

Even with a high precision Hall probe the relative alignment of the probe and the magnet is still crucial for a precise measurement of the field. The solenoidal field (Fig. 4) itself offers the possibility to align the used linear stage and Hall probe relative to the magnetic field of the PMS. In its transverse plane at the position of the maximum longitudinal field it has only a longitudinal field component. This fact can be used to align the axes of the Hall probe. At the longitudinal position of the zero-crossing of the magnetic field all field components are equal to zero. These two points define the
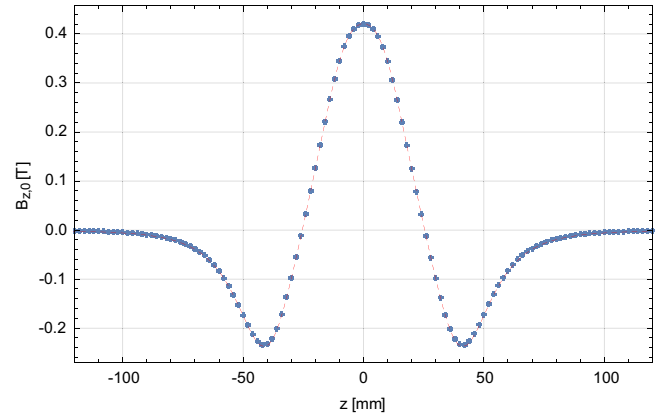

Fig. 4. Measured (blue dots, with error bars) and simulated (red dashed) on-axis magnetic field $B_{z,0}$. (For interpretation of the references to color in this figure caption, the reader is referred to the web version of this paper.)

symmetry axis of the solenoid which can be used to align the PMS with respect to the longitudinal axis of the linear stage. Because already small deviations of the alignment can cause big deviations of the measured from the simulated magnetic field a post-processing alignment is necessary to compare simulations and measurements.

In order to fit the measured and simulated field a simple least-square routine was chosen which rotates and shifts the simulated field with respect to the measured and minimizes the deviations of the two compared fields. The rotations and shifts were introduced to our simulation tool.

The final result for a measured and post-processed on-axis field profile is shown in Fig. 4. The conformity of the measured and simulated (flawless wedges) field is very high.

5. Conclusion

We were able to develop an analytical and fast magnetic field simulation tool which is very general and not limited to solenoidal fields. The same holds for the sorting algorithm. It connects the field quality directly with the change of beam quality due to the deformed field. Furthermore the comparison between measurements and simulations was successful despite the challenging magnetic field measurement.

References

[1] Jason R. Dwyer, Christoph T. Hebeisen, Ralph. Ernstorfer, Maher. Harb, Vatche B. Deyirmenjian, Robert E. Jordan, R.J. Dwayne Miller, Philosophical Transactions of the Royal Society A 364 (January) (2006) 741.

[2] Stephanie Manz, Albert Casandruc, Dongfang Zhang, Yinpeng Zhong, Rolf A. Loch, Alexander Marx, Taisuke Hasegawa, Lai Chung Liu, Shima Bayesteh, Hossein Delsim-Hashemi, Matthias Hoffmann, Matthias Felber, Max Hachmann, Frank Mayet, Julian Hirscht, Sercan Keskin, Masaki Hada, Sascha W. Epp, Klaus Floettmann, R.J. Dwayne Miller, Faraday Discuss 177 (January) (2015) 476.

[3] Benno Zeitler, Irene Dornmair, Tim Gehrke, Mikheil Titberidze, Andreas R. Maier, Bernhard Hidding, Klaus Floettmann, Florian Gruener. Merging conventional and laser wakefield accelerators, in: Proceedings of the SPIE, vol. 8779, 2013.

[4] Tim Gehrke, Design of permanent magnetic solenoids for REGAE (Master's thesis), University of Hamburg, Germany, 2013.

[5] S. Kirkpatrick, C.D. Gelatt, M.P. Vecchi, Science 220 (May (4598)) (1983) 671.

[6] B. Faatz, J. Pflueger, Magnet Sorting for the TTF-FEL Undulator using Simulated Annealing, TESLA FEL Report, 1999–01.

[7] Klaus Floettmann, Astra, URL ⟨http://www.desy.de/mpyflo⟩, 2014.

[8] Metrolab Technology SA, Three-axis Magnetometers THM1176 and TFM1186: user's manual, URL ⟨http://thm1176.metrolab.com⟩, 2014.